

Knowledge Graph Reasoning with Relational Directed Graph

Yongqi Zhang¹ Quanming Yao^{1,2}

¹4Paradigm Inc.

²Department of Electronic Engineering, Tsinghua University
zhangyongqi@4paradigm.com, qyaoaa@mail.tsinghua.edu.cn

Abstract

Reasoning on the knowledge graph (KG) aims to infer new facts from existing ones. Methods based on the relational path in the literature have shown strong, interpretable, and inductive reasoning ability. However, the paths are naturally limited in capturing complex topology in KG. In this paper, we introduce a novel relational structure, i.e., relational directed graph (r-digraph), which is composed of overlapped relational paths, to capture the KG’s structural information. Since the digraph exhibits more complex structure than paths, constructing and learning on the r-digraph are challenging. Here, we propose a variant of graph neural network, i.e., RED-GNN, to address the above challenges by learning the *RE*lational *D*igraph with a variant of GNN. Specifically, RED-GNN recursively encodes multiple r-digraphs with shared edges and selects the strongly correlated edges through query-dependent attention weights. We demonstrate the significant gains on reasoning both KG with unseen entities and incompleteness KG benchmarks by the r-digraph, the efficiency of RED-GNN, and the interpretable dependencies learned on the r-digraph.

1 Introduction

Knowledge graph (KG), which contains the interactions among real-world objects, peoples, concepts, etc., brings much connection between artificial intelligence and human knowledge [1, 13]. The interactions are formed as facts with the triple form (*subject entity*, *relation*, *object entity*) to indicate the relation between entities. The real-world KGs are large and highly incomplete [35, 13], thus inferring new facts is challenging. KG reasoning simulates such a process to deduce new facts from existing facts [4]. In this paper, we focus on learning the relational structures for reasoning on the queries in the form of (*subject entity*, *relation*, ?).

Over the last decade, triple-based models have gained much attention to learn knowledge in KGs [35]. These models directly reason on triples with the entity and relation embeddings, such as TransE [3], ConvE [7], ComplEx [31], RotatE [28], QuatE [41] etc. Since the triples are independently learned, they cannot explicitly capture the structural information [21, 36, 39, 29], i.e., the local structures around the query triples, which can be used as evidence for KG reasoning, based on the Gaifman’s locality theorem [21].

Relational path is the first attempt to capture the structural information for reasoning [18]. DeepPath [36], MINERVA [6] and M-walk [27] use reinforcement learning (RL) to sample relational paths that have strong correlation with the queries. Due to the sparse properties of KGs, the RL approaches are hard to train on large-scale KGs [4]. PathCon [34] samples all the relational paths between the entities and use attention mechanism to weight the different paths, but is expensive for the entity query tasks. The rule-based methods, such as RuleN [20], Neural LP [39], DRUM [25] and RNNLogic [23], generalize the relational paths as logical rules, which learn to infer relations by

logical composition of relations, and can provide interpretable insights. Besides, the logical rules can be transferred to previously unseen entities that are common in real-world applications, which cannot be handled by the triple-based models [39, 25].

Subgraphs can naturally be more informative than paths in capturing the structural information [1]. Their effectiveness has been empirically verified in, e.g., graph-based recommendation [42] and node representation learning [9]. With the success of graph neural network (GNN) [8, 15, 37] in modeling graph-structured data, GNN has been introduced to capture the subgraph structures in KG. R-GCN [26] and CompGCN [32] propose to update the representations of entities by aggregating all the 1-hop neighbors on KG in each layer. However, it cannot distinguish the structural dependency of different neighbors and cannot be interpretable. DPMPN [38] learns to reduce the size of subgraph for reasoning on large-scale KGs by preserving the most probable entities for a given query rather than learning the specific local structures. Recently, GraIL [29] proposes to predict relation from the local enclosing subgraph structure and shows the inductive ability of subgraph. However, it suffers from both effectiveness and efficiency problems due to the limitation of the enclosing subgraph.

Inspired by the interpretable and transferable abilities of path-based methods and the structure preserving property of subgraphs, we introduce a novel relational structure into KG called r-digraph. The r-digraphs generalize relational paths to subgraphs by preserving the overlapped relational paths and the structures of relations for reasoning. Different from the relational paths that have simple structures, how to efficiently construct and learn from the r-digraphs are challenging since directly computing on each r-digraph is very expensive for reasoning the query. Inspired by solving computation costs in overlapping sub-problems using dynamic programming, we propose RED-GNN, an efficient learning framework for the *RE*lational *D*igraph with a variant of GNN [8]. Empirically, RED-GNN shows significant gains over the state-of-the-art reasoning methods in both benchmarks for KG with unseen entities and incomplete KG. Besides, the training and inference processes are efficient, and the learned structures are interpretable.

2 Related Works

A knowledge graph is in form of $\mathcal{K} = \{\mathcal{V}, \mathcal{R}, \mathcal{F}\}$, where \mathcal{V} , \mathcal{R} and $\mathcal{F} = \{(e_s, r, e_o) | e_s, e_o \in \mathcal{V}, r \in \mathcal{R}\}$ are the sets of entities, relations and fact triples, respectively. Let e_q be query entity, r_q be query relation, and e_a be answer entity. Given the query $(e_q, r_q, ?)$, the reasoning task is to predict the missing answer entity e_a . Generally, all the entities in \mathcal{V} are candidates for e_a [4, 6, 39].

The key for KG reasoning is to capture the local evidence, such as relational paths or subgraphs, around the queries. In this part, we introduce the path-based methods and GNN-based methods that leverage structures in \mathcal{F} for reasoning.

2.1 Path-based methods

Relational path is formed by a set of triples that are sequentially connected as in Def.1. It is more informative than single triple since it can provide interpretable results and transfer to unseen entities.

Definition 1 (Relational path [19, 36]). *The relational path with length L is a set of L consecutive triples $(e_0, r_1, e_1), (e_1, r_2, e_2), \dots, (e_{L-1}, r_L, e_L)$, that are connected head-to-tail in sequence.*

The path-based methods learn to predict the triple (e_q, r_q, e_a) by a set of relational paths as local evidence. DeepPath [36] learns to generate the relational path from e_q to e_a by reinforcement learning (RL). To improve the efficiency, MINERVA [6] and M-walk [27] learn to generate from e_q with multiple paths by RL. The scores are indicated by the arrival frequency on different e_a 's. Due to the complex structure of KG, the reward is very sparse, making it hard to train the RL models [4]. PathCon [34] samples all the paths connecting the two entities to predict the relation between them, which is expensive for the reasoning task (e_q, r_q, e_a) .

Instead of directly using paths, the rule-based methods learn logical rules as a generalized form of relational paths. The logical rules are formed with the composition of a set of relations to infer a specific relation to provide better interpretation and can be transferred to unseen entities. The rules can be learned by either the discrete mining like RuleN [20], EM algorithm like RNNLogic [23], or end-to-end training, such as Neural LP [39] and DRUM [25], to generate highly correlated relational paths between e_q and e_a . The rules can provide logical interpretation and transfer to unseen entities. However, the rules can only capture the sequential evidences, thus cannot learn more complex patterns such as the subgraph structures.

2.2 GNN-based methods

As in the introduction, the subgraphs can naturally preserve richer information than the relational paths. All the relational paths are sampled from some local subgraphs. Thus, they naturally loss some structural information in KGs, e.g., how multiple entities and edges are connected. GNN has shown strong power in modeling the graph structured data [1]. This inspires recent works, such as R-GCN [26] and CompGCN [32], extending GNN on KG to aggregate the entities' and relations' representations under the message passing framework [8] as

$$\mathbf{h}_{e_o}^\ell = \delta\left(\mathbf{W}^\ell \cdot \sum_{(e_s, r, e_o) \in \mathcal{F}} \phi(\mathbf{h}_{e_s}^{\ell-1}, \mathbf{h}_r^\ell)\right), \quad (1)$$

which aggregates over the message on the 1-hop neighbor edges $(e_s, r, e_o) \in \mathcal{F}$ of entity e_o with dimension d . $\phi(\cdot, \cdot)$ is the message function, $\mathbf{W}^\ell \in \mathbb{R}^{d \times d}$ is a weighting matrix and δ is the activation function. After L layers, the representations \mathbf{h}_e^L capturing the local structures of entities $e \in \mathcal{V}$ jointly work with a scoring function to score the triples. Since the aggregation function aggregates information of all the neighbors and is independent with the query, R-GCN and CompGCN cannot capture the explicit structures used for reasoning specific queries and are not interpretable.

Instead of using all the neighborhoods, DPMPN [38] designs one GNN to aggregate the embeddings of entities, and another GNN to dynamically expand and prune the inference subgraph from the query entity e_q . A query-dependent attention is applied over the sampled entities for pruning. This approach shows explainable reasoning process by the attention flow on the pruned subgraph but still requires embeddings to guide the pruning, thus cannot be generalized to unseen entities. Besides, it cannot capture the explicit subgraph structure supporting a given query triple. xERTR [10] extends DPMPN for reasoning future triples in temporal KGs.

Recently, GraIL [29] proposes to extract the enclosing subgraph $\mathcal{G}_{(e_q, e_a)}$ between the query entity e_q and answer entity e_a . To learn the enclosing subgraph, the relational GNN [26] with query-dependent attention is applied over the edges in $\mathcal{G}_{(e_q, e_a)}$ to control the importance of edges for different queries. After L layers' aggregation, the graph-level representations aggregating all the entities $e \in \mathcal{V}$ in the subgraph are used to score the triple (e_q, r_q, e_a) . Since the subgraphs need to be explicitly extracted and scored for different triples, the computation cost is very high.

3 Relational Digraph

The relational paths, especially the logical rules, have shown strong reasoning ability on KGs [6, 39, 25] to offer interpretable results and transfer to unseen entities. However, they are limited in capturing more complex dependencies in KG since they are sampled from the local subgraphs. GNN-based methods can learn different subgraph structures. But none of the existing methods can efficiently learn the subgraph structures that are both interpretable and transferable to unseen entities like rules. Hence, we are motivated to define a new kind of structure, i.e., r-digraph, to explore the structural dependency by generalizing relational paths. In subsequent Sect.4, we show how GNNs can be tailor-made to efficiently and effectively learn from the r-digraphs.

Before defining r-digraph, we first introducing a special type of digraph in Def.2.

Definition 2 (Layered *st*-graph [2]). *The layered st-graph is a directed graph with exactly one source node (s) and one sink node (t). All the edges are directed, connecting nodes between consecutive layers and pointing from lower layer to higher one.*

Here, we adopt the general approaches to augment the triples with reverse and identity relations [32, 25, 40]. Then, all the relational paths with length less than or equal to L between e_q and e_a can be represented as $e_q \rightarrow_{r^1} \rightarrow_{r^2} \cdots \rightarrow_{r^L} e_a$ with length L . In this way, they can be formed as paths in a layered *st*-graph, with the single source entity e_q and single sink entity e_a . Such a structure preserves all the relational paths between e_q and e_a up to length L , and maintains the subgraph structure. Based on this observation, we define r-digraph in Def. 3.

Definition 3 (r-digraph). *The r-digraph $\mathcal{G}_{e_q, e_a|L}$ is a layered st-graph with the source entity e_q and the sink entity e_a . The entities in the same layer are different with each other. Any path pointing from e_q to e_a in the r-digraph is a relational path $e_q \rightarrow_{r^1} \rightarrow_{r^2} \cdots \rightarrow_{r^L} e_a$ with length L , where r^ℓ connects an entity in the $\ell-1$ -layer to an entity in ℓ -layer. We define $\mathcal{G}_{e_q, e_a|L} = \emptyset$ if there is no relational path connecting e_q and e_a with length L .*

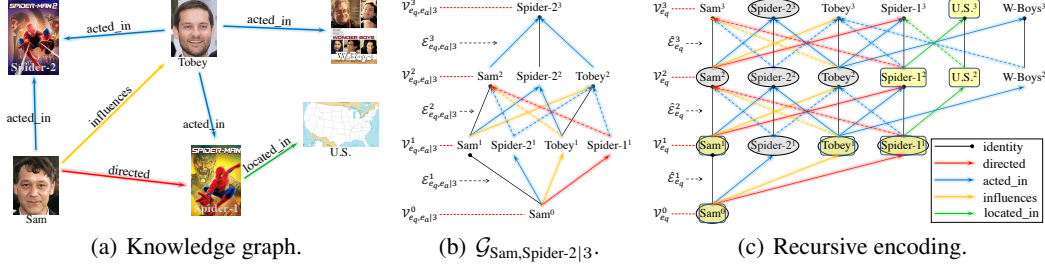


Figure 1: Graphical illustration. In (c), the subgraph formed by the gray ellipses is $\mathcal{G}_{\text{Sam}, \text{Spider-2}|3}$ and the subgraph formed by the yellow rectangles is $\mathcal{G}_{\text{Sam}, \text{U.S.}|3}$. Dashed edges mean the reverse relations of corresponding color (best viewed in color).

Fig.1(b) provides an example of r-digraph $\mathcal{G}_{\text{Sam}, \text{Spider-2}|3}$, which can be used infer the new triple (*Sam*, *directed*, *Spider-2*), in the exemplar KG in Fig.1(a). Inspired by the reasoning ability of relational paths [6, 39, 25], we aim to exploit the r-digraph for KG reasoning. However, different from the relational paths which have simple structures, how to efficiently construct and how to effectively learn from the r-digraph are challenging.

In the sequel, $\mathcal{E}_{e_q, e_a|L}^\ell$ are edges and $\mathcal{V}_{e_q, e_a|L}^\ell = \{e_o | (e_s, r, e_o) \in \mathcal{E}_{e_q, e_a|L}^\ell\}$ are entities in the ℓ -th layer of the r-digraph $\mathcal{G}_{e_q, e_a|L} = \mathcal{E}_{e_q, e_a|L}^1 \otimes \dots \otimes \mathcal{E}_{e_q, e_a|L}^L$ with $\ell = 1 \dots L$. \otimes denotes the layer-wise connection. We define $\mathcal{G}_{e_{q1}, e_{a1}|L} \cup \mathcal{G}_{e_{q2}, e_{a2}|L} = (\mathcal{E}_{e_{q1}, e_{a1}|L}^1 \cup \mathcal{E}_{e_{q2}, e_{a2}|L}^1) \otimes \dots \otimes (\mathcal{E}_{e_{q1}, e_{a1}|L}^L \cup \mathcal{E}_{e_{q2}, e_{a2}|L}^L)$. Given the query entity e_q , we denote $\hat{\mathcal{E}}_{e_q}^\ell$ as the set of out-edges and $\mathcal{V}_{e_q}^\ell$ as the set of entities visible in ℓ steps walking from e_q . $\mathcal{E}_{e_q, e_a|L}^\ell$, $\mathcal{V}_{e_q, e_a|L}^\ell$ and $\hat{\mathcal{E}}_{e_q}^\ell$, $\mathcal{V}_{e_q}^\ell$ are graphically shown in Fig.1.

4 RED-GNN

To encode the r-digraph $\mathcal{G}_{e_q, e_a|L}$, a simple solution is to construct it first and run message passing (1) as in Alg.1. For construction, we get the out-edges and entities of e_q in step 2-4. If $e_a \notin \mathcal{V}_{e_q}^L$, $\mathcal{G}_{e_q, e_a|L}$ will be empty and we set the representation as $\mathbf{0}$ in step 5. For $\mathcal{G}_{e_q, e_a|L}$ that is not empty, we construct it backward from e_a in step 6-8. After the construction, we run message passing on $\mathcal{E}_{e_q, e_a|L}^\ell$ layer-by-layer in step 10. Since e_a is the single sink entity in $\mathcal{G}_{e_q, e_a|L}$, the final layer representation $\mathbf{h}_{e_a}^L(e_q, r_q)$ is used as subgraph representation to encode the structure of $\mathcal{G}_{e_q, e_a|L}$.

Algorithm 1 Message passing on single r-digraph

Require: a knowledge graph $\mathcal{K} = \{\mathcal{V}, \mathcal{R}, \mathcal{F}\}$, query triple (e_q, r_q, e_a) , depth L .

- 1: initialize $\mathbf{h}_{e_q}^0(e_q, r_q) = \mathbf{0}$ and the entity sets $\mathcal{V}_{e_q, e_a|L}^0 = \mathcal{V}_{e_q}^0 = \{e_q\}$, $\mathcal{V}_{e_q, e_a|L}^L = \{e_a\}$;
- 2: **for** $\ell = 1, 2, \dots, L$ **do**
- 3: get the ℓ -hop out-edges $\hat{\mathcal{E}}_{e_q}^\ell = \{(e_s, r, e_o) \in \mathcal{F} | e_s \in \mathcal{V}_{e_q}^{\ell-1}\}$ and entities $\mathcal{V}_{e_q}^\ell = \{e_o | (e_s, r, e_o) \in \hat{\mathcal{E}}_{e_q}^\ell\}$;
- 4: **end for**
- 5: **if** $\mathcal{V}_{e_q}^L \cap \mathcal{V}_{e_q, e_a|L}^L = \emptyset$ **return** $\mathbf{h}_{e_q}^L(e_q, r_q) = \mathbf{0}$;
- 6: **for** $\ell = L, L-1, \dots, 1$ **do**
- 7: get the ℓ -layer edges: $\mathcal{E}_{e_q, e_a|L}^\ell = \{(e_s, r, e_o) \in \hat{\mathcal{E}}_{e_q}^\ell | e_o \in \mathcal{V}_{e_q, e_a|L}^\ell\}$ and the $\ell-1$ -layer entities: $\mathcal{V}_{e_q, e_a|L}^{\ell-1} = \{e_s | (e_s, r, e_o) \in \mathcal{E}_{e_q, e_a|L}^\ell\}$;
- 8: **end for**
- 9: **for** $\ell = 1, 2, \dots, L$ **do**
- 10: message passing: $\mathbf{h}_e^\ell(e_q, r_q) = \delta(\mathbf{W}^\ell \cdot \sum_{(e_s, r, e) \in \mathcal{E}_{e_q, e_a|L}^\ell} \phi(\mathbf{h}_{e_s}^{\ell-1}(e_q, r_q), \mathbf{h}_r^\ell))$, for $e \in \mathcal{V}_{e_q, e_a|L}^\ell$;
- 11: **end for**
- 12: **return** $\mathbf{h}_{e_a}^L(e_q, r_q)$.

However, Alg.1 is very expensive. First, given a query $(e_q, r_q, ?)$, we need to do this algorithm for $|\mathcal{V}|$ different triples with different answering entities $e_a \in \mathcal{V}$. Second, three loops are required in this algorithm. It needs $O(|\mathcal{V}| \cdot (\min(\bar{D}^L, |\mathcal{F}|L) + d\bar{E}L))$ time (details in Appendix B) to predict a given query $(e_q, r_q, ?)$, where \bar{D} is the average degree of entities in \mathcal{V} and \bar{E} is the average number

of edges in $\mathcal{E}_{e_q, e_a|L}^\ell$. These limitations also exist in PathCon [34] and GraIL [29] (see Appendix D). To improve efficiency, we propose to encode multiple r-digraphs recursively in Sect.4.1.

4.1 Recursive r-digraph encoding

In Alg.1, when enumerating (e_q, r_q, e_a) with different $e_a \in \mathcal{V}$ for the same query $(e_q, r_q, ?)$, the neighboring edges $\hat{\mathcal{E}}_{e_q}^\ell, \ell = 1 \dots L$ of e_q are shared. Thus, we have the following observation:

Proposition 4.1. *The set of edges $\hat{\mathcal{E}}_{e_q}^\ell$ visible from e_q by ℓ -steps is the union of the ℓ -th layer edges in the r-digraphs between e_q and all the entities $e_a \in \mathcal{V}$, namely $\hat{\mathcal{E}}_{e_q}^\ell = \cup_{e_a \in \mathcal{V}} \mathcal{E}_{e_q, e_a|L}^\ell$.*

Prop.4.1 indicates that the ℓ -th layer edges $\mathcal{E}_{e_q, e_a|L}^\ell$ with different entities e_a share the same set of edges in $\hat{\mathcal{E}}_{e_q}^\ell$. Inspired by saving computation costs in overlapping sub-problems using dynamic programming, the r-digraph between e_q and any entity e_o can be recursively constructed as

$$\mathcal{G}_{e_q, e_o|L} = \cup_{(e_s, r, e_o) \in \hat{\mathcal{E}}_{e_q}^\ell} \mathcal{G}_{e_q, e_s|L-1} \otimes \{(e_s, r, e_o) \in \hat{\mathcal{E}}_{e_q}^\ell\}. \quad (2)$$

Once the representations of $\mathcal{G}_{e_q, e_s|L-1}$ for different entities e_s in the $\ell-1$ -th layer are ready, we can encode $\mathcal{G}_{e_q, e_o|L}$ by combining $\mathcal{G}_{e_q, e_s|L-1}$ with the shared edges $(e_s, r, e_o) \in \hat{\mathcal{E}}_{e_q}^\ell$ in the ℓ -th layer. Based on Prop.4.1 and (2), we are motivated to recursively encode multiple r-digraphs with the shared edges in $\hat{\mathcal{E}}_{e_q}^\ell$ layer by layer. The full process is in Alg.2.

Algorithm 2 RED-GNN: recursive r-digraph encoding.

Require: a knowledge graph $\mathcal{K} = \{\mathcal{V}, \mathcal{R}, \mathcal{F}\}$, query $(e_q, r_q, ?)$, depth L .

- 1: initialize $\mathbf{h}_{e_q}^0(e_q, r_q) = \mathbf{0}$ and the entity set $\mathcal{V}_{e_q}^0 = \{e_q\}$;
 - 2: **for** $\ell = 1 \dots L$ **do**
 - 3: collect the ℓ -hop edges $\hat{\mathcal{E}}_{e_q}^\ell = \{(e_s, r, e_o) \in \mathcal{F} | e_s \in \mathcal{V}_{e_q}^{\ell-1}\}$ and entities $\mathcal{V}_{e_q}^\ell = \{e_o | (e_s, r, e_o) \in \hat{\mathcal{E}}_{e_q}^\ell\}$;
 - 4: message passing: $\mathbf{h}_{e_o}^\ell(e_q, r_q) = \delta(\mathbf{W}^\ell \cdot \sum_{(e_s, r, e_o) \in \hat{\mathcal{E}}_{e_q}^\ell} \phi(\mathbf{h}_{e_s}^{\ell-1}(e_q, r_q), \mathbf{h}_r^\ell))$, for $e_o \in \mathcal{V}_{e_q}^\ell$;
 - 5: **end for**
 - 6: assign $\mathbf{h}_{e_a}^L(e_q, r_q) = \mathbf{0}$ for all $e_a \notin \mathcal{V}_{e_q}^L$;
 - 7: **return** $\mathbf{h}_{e_a}^L(e_q, r_q)$ for all $e_a \in \mathcal{V}$.
-

Initially, only e_q is visible in $\mathcal{V}_{e_q}^0$. In the ℓ -th layer, we collect the edges $\hat{\mathcal{E}}_{e_q}^\ell$ and entities $\mathcal{V}_{e_q}^\ell$ in step 3. Then, the message passing is constrained in $\mathcal{E}_{e_q}^\ell$ to get the representations for $e_o \in \mathcal{V}_{e_q}^\ell$. Finally, the representations $\mathbf{h}_{e_a}^L(e_q, r_q)$, encoding $\mathcal{G}_{e_q, e_a|L}$ for all the entities e_a , are returned in step 7. The recursive encoding can be more efficient with shared edges in $\hat{\mathcal{E}}_{e_q}^\ell$ and fewer loops, It takes time $O(\min(\bar{D}^L, |\mathcal{F}|L) \cdot d)$, $d \ll |\mathcal{V}|$. And it learns the same representations as Alg.1 under Prop.4.2.

Proposition 4.2. *Given the same triple (e_q, r_q, e_a) , the structures encoded in $\mathbf{h}_{e_a}^L(e_q, r_q)$ by Algorithm 1 and Algorithm 2 are identical.*

4.2 Learning essential information for query

Up to here, the information of query relation r_q has not yet been addressed. To learn query-dependent representation of the r-digraphs, we specify the aggregation function as

$$\mathbf{h}_{e_o}^\ell(e_q, r_q) = \delta\left(\mathbf{W}^\ell \cdot \sum_{(e_s, r, e_o) \in \hat{\mathcal{E}}_{e_q}^\ell} \alpha_{e_s, r, r_q}^\ell (\mathbf{h}_{e_s}^{\ell-1}(e_q, r_q) + \mathbf{h}_r^\ell)\right). \quad (3)$$

To discover important edges, especially relations, in each layer, r_q is encoded into the attention weight $\alpha_{e_s, r, r_q}^\ell$ on each edge (e_s, r, e_o) as

$$\alpha_{e_s, r, r_q}^\ell = \sigma\left((\mathbf{w}_\alpha^\ell)^\top \text{ReLU}(\mathbf{W}_\alpha^\ell \cdot (\mathbf{h}_{e_s}^{\ell-1}(e_q, r_q) \oplus \mathbf{h}_r^\ell \oplus \mathbf{h}_{r_q}^\ell))\right), \quad (4)$$

with $\mathbf{w}_\alpha^\ell \in \mathbb{R}^{d_\alpha}$, $\mathbf{W}_\alpha^\ell \in \mathbb{R}^{d_\alpha \times 3d}$, and \oplus is the concatenation operator. Sigmoid function σ is used rather than softmax attention [33] to ensure multiple edges can be selected in the same neighborhood.

After L layers' aggregation in (3), the representations $\mathbf{h}_{e_a}^L(e_q, r_q)$ can encode essential information for scoring (e_q, r_q, e_a) . Hence, we design a simple scoring function $f(e_q, r_q, e_a) = \mathbf{w}^\top \mathbf{h}_{e_a}^L(e_q, r_q)$ with $\mathbf{w} \in \mathbb{R}^d$. We associate the multi-class log-loss [17] with each training triple (e_q, r_q, e_a) , i.e.,

$$\mathcal{L} = \sum_{(e_q, r_q, e_a) \in \mathcal{T}_{\text{tra}}} \left(-f(e_q, r_q, e_a) + \log\left(\sum_{\forall e \in \mathcal{V}} e^{f(e_q, r_q, e)}\right) \right). \quad (5)$$

The first part in (5) is the score of the positive triple (e_q, r_q, e_a) in the training set \mathcal{T}_{tra} , and the second part contains the scores of all triples with the same query $(e_q, r_q, ?)$. The model parameters $\Theta = \{\{\mathbf{W}^\ell\}, \{\mathbf{w}_\alpha^\ell\}, \{\mathbf{W}_\alpha^\ell\}, \{\mathbf{h}_r^\ell\}, \mathbf{w}\}$ are randomly initialized and are optimized by minimizing (5) with stochastic gradient descent [14].

Theorem 4.3. *Given a triple (e_q, r_q, e_a) , let \mathcal{P} be a set of relational paths $e_q \rightarrow_{r_1^1} \rightarrow_{r_2^2} \cdots \rightarrow_{r_i^L} e_a$, which have strong correlation with (e_q, r_q, e_a) . Denote $\mathcal{G}_{\mathcal{P}}$ as the r -digraph constructed by \mathcal{P} . There exists a parameter setting Θ and a threshold $\theta \in (0, 1)$ for RED-GNN that $\mathcal{G}_{\mathcal{P}}$ can equals to the subgraph, whose edges have attention weights $\alpha_{e_s, r, r_q}^\ell > \theta$, in $\mathcal{G}_{e_q, e_a|L}$.*

We provide Theorem 4.3 which means that if a set of relational paths are strongly correlated with the query triple, they can be identified by the attention weights in RED-GNN.

5 Experiments

All the experiments are written in Python with PyTorch framework [22] and run on an RTX 2080Ti GPU with 11GB memory.

5.1 Reasoning on KG with unseen entities

Reasoning on KG with unseen entities recently becomes a hot topic [25, 29, 39] as there are emerging new entities in the real-world scenarios, such as new users and new concepts. Transferring to unseen entities requires the model to understand how to infer relations based on the local evidences ignoring the identity of entities.

Setup. We follow the general setting [25, 29, 39] that reasons on a KG with unseen entities. Specifically, the training and testing contain two KGs $\mathcal{K}_{\text{tra}} = \{\mathcal{V}_{\text{tra}}, \mathcal{R}, \mathcal{F}_{\text{tra}}\}$ and $\mathcal{K}_{\text{tst}} = \{\mathcal{V}_{\text{tst}}, \mathcal{R}, \mathcal{F}_{\text{tst}}\}$, with the same set of relations but disjoint sets of entities. Three sets of triples $\mathcal{T}_{\text{tra}}/\mathcal{T}_{\text{val}}/\mathcal{T}_{\text{tst}}$, augmented with reverse relation, are provided. \mathcal{F}_{tra} is used to predict \mathcal{T}_{tra} and \mathcal{T}_{val} for training and validation, respectively. In testing, \mathcal{F}_{tst} is used to predict \mathcal{T}_{tst} . Same as [25, 29, 39], we use the filtered ranking metrics, i.e., mean reciprocal rank (MRR), Hit@1 and Hit@10 [3], to indicate better performance with larger values. We use the benchmark dataset in [29], created on WN18RR [7], FB15k237 [30] and NELL-995 [36]. Each dataset includes four versions with different groups of triples. The hyper-parameters, including learning rate, weight decay, dropout, batch size, dimension d , number of layers L and activation function, are selected by the MRR metric on \mathcal{T}_{val} with maximum training epochs of 50. More details of the setup are in Appendix A.2.

Baselines. Since training and testing contain disjoint sets of entities, all the methods requiring the entity embeddings cannot be applied here [25, 29]. We mainly compare with four methods: 1) RuleN [20], the discrete rule induction method; 2) Neural-LP [39], the first differentiable method for rule learning; 3) DRUM [25], an improved work of Neural-LP [39]; and 4) GraIL [29], which designs the enclosing subgraph for inductive reasoning. MINERVA [6], PathCon [34] and RNNLogic [23] can potentially work on this setting but lack of source code on it, thus not compared.

Results. The performance is shown in Tab.1. First, GraIL is the worst among all the methods since the enclosing subgraphs does not learn well of the relational structures that can be generalized to unseen entities. Second, there is not absolute winner among the rule-based methods as different rules adapt differently to these datasets. In comparison RED-GNN outperforms the baselines across all of the benchmarks. Based on Theorem 4.3, the attention weights can help to adaptively learn correlated relational paths for different datasets, and preserving the structural patterns at the same time. The results of Hit@1 and Hit@10 are provided in Appendix A.2 due to space limitation. In some cases, the Hit@10 of RED-GNN is slightly worse than the rule-based methods since it may overfit to the top-ranked samples.

Table 1: Results on KG with unseen entities. Best performance is indicated by the bold face numbers.

metric	methods	WN18RR				FB15k-237				NELL-995			
		V1	V2	V3	V4	V1	V2	V3	V4	V1	V2	V3	V4
MRR	RuleN	.668	.645	.368	.624	.363	.433	.439	.429	.615	.385	.381	.333
	Neural LP	.649	.635	.361	.628	.325	.389	.400	.396	.610	.361	.367	.261
	DRUM	.666	.646	.380	.627	.333	.395	.402	.410	.628	.365	.375	.273
	GraIL	.627	.625	.323	.553	.279	.276	.251	.227	.481	.297	.322	.262
	RED-GNN	.701	.690	.427	.651	.369	.469	.445	.442	.637	.419	.436	.363

Table 2: Results on incomplete KG. $H@1$ and $H@10$ are short for $\text{Hit}@1$ and $\text{Hit}@10$ in percentage. Best performance is indicated by the bold face numbers. * is copied from best results in their paper.

type	models	Family			UMLS			WN18RR			FB15k-237			NELL-995		
		MRR	H@1	H@10	MRR	H@1	H@10	MRR	H@1	H@10	MRR	H@1	H@10	MRR	H@1	H@10
triple	RotatE	.921	86.6	98.8	.925	86.3	99.3	.477	42.8	57.1	.337	24.1	53.3	.508	44.8	60.8
	QuatE	.941	89.6	99.1	.944	90.5	99.3	.480	44.0	55.1	.350	25.6	53.8	.533	46.6	64.3
path	MINERVA	.885	82.5	96.1	.825	72.8	96.8	.448	41.3	51.3	.293	21.7	45.6	.513	41.3	63.7
	Neural LP	.924	87.1	99.4	.745	62.7	91.8	.435	37.1	56.6	.252	18.9	37.5	out	of	memory
	DRUM	.934	88.1	99.6	.813	67.4	97.6	.486	42.5	58.6	.343	25.5	51.6	out	of	memory
	RNNLogic*	—	—	—	.842	77.2	96.5	.483	44.6	55.8	.344	25.2	53.0	—	—	—
GNN	CompGCN	.933	88.3	99.1	.927	86.7	99.4	.479	44.3	54.6	.355	26.4	53.5	out	of	memory
	DPMPN	.981	97.4	98.1	.930	89.9	98.2	.482	44.4	55.8	.369	28.6	53.0	.513	45.2	61.5
	RED-GNN	.992	98.8	99.7	.964	94.6	99.0	.533	48.5	62.4	.364	27.3	.544	.543	47.6	65.1

5.2 Reasoning on incomplete KG

Reasoning on incomplete KGs is another general setting in the literature, i.e., KG completion [35]. It evaluates the models’ ability to learn the patterns on an incomplete KG.

Setup. In this setting, a KG $\mathcal{K} = \{\mathcal{V}, \mathcal{R}, \mathcal{F}\}$ and the query triples $\mathcal{T}_{val}/\mathcal{T}_{test}$, augmented with reverse relation, are given. For the triple-based method, triples in \mathcal{F} are used for training and $\mathcal{T}_{val}/\mathcal{T}_{test}$ are used for inference. For the others, $3/4$ of the triples in \mathcal{F} are used to extract paths/subgraphs to predict the remaining $1/4$ triples in training, and the full set \mathcal{F} is then used to predict $\mathcal{T}_{val}/\mathcal{T}_{test}$ in inference [39, 25]. We use the same ranking metrics in Section 5.1, namely MRR, $\text{Hit}@1$ and $\text{Hit}@10$. Five well-known¹ benchmarks are used including Family [16], UMLS [16], WN18RR [7], FB15k237 [30] and NELL-995 [36]. The setting of hyper-parameters of RED-GNN are same as those in Section 5.1. More details are provided in Appendix A.3.

Baselines. We compare with the triple-based methods RotatE [28] and QuatE [41]; the path-based methods MINERVA [6], Neural LP [39], DRUM [25] and RNNLogic [23]; and the GNN-based methods CompGCN [32] and DPMPN [38]. RuleN [20] is not compared here since it has been shown to be worse than DRUM [25] and RNNLogic [23] in this setting. GraIL [29] is not compared since it is computationally intractable (see Section 5.3).

Results. As in Tab.2, the triple-based methods are better than the path-based ones on Family and UMLS, and is comparable with DRUM and RNNLogic on WN18RR, FB15k-237. The entity embeddings can implicitly preserve local information around entities, while the path-based methods may lose the structural patterns. CompGCN performs similar as the triple-based methods since it mainly relies on the aggregated embeddings and the decoder scoring function. Neural LP, DRUM and CompGCN run out of memory on NELL-995 with 74k entities due to the use of full adjacency matrix. For DPMPN, the entities in the pruned subgraph is more informative than that in CompGCN, thus has better performance. For RED-GNN, it is the runner up on FB15k-237 and the best on the other benchmarks. These demonstrate that the r-digraph can not only transfer well to unseen entities, but also capture the important patterns in incomplete KGs without using entity embeddings.

5.3 Running time analysis

We compare the running time of different methods in this part. We show the training time and the inference time on \mathcal{T}_{test} for each method in Fig 2(a) and 2(c), and learning curves in Fig 2(b) and 2(d).

¹With the versions in <https://github.com/alisadeghian/DRUM/tree/master/datasets> and <https://github.com/thunlp/OpenKE/tree/OpenKE-PyTorch/benchmarks/NELL-995>.

Table 3: Comparison of different variants of RED-GNN.

methods	WN18RR (V1)			FB15k-237 (V1)			NELL (V1)		
	MRR	Hit@1	Hit@10	MRR	Hit@1	Hit@10	MRR	Hit@1	Hit@10
Attn-w.o.- r_q	.659	58.6	78.3	.268	20.1	37.6	.517	40.5	73.4
RED-Alg.1	.683	63.1	79.6	.311	23.2	45.3	.563	48.5	75.8
RED-GNN	.701	65.3	79.9	.369	30.2	48.3	.637	52.5	86.6

For reasoning on KG with unseen entities, we compare RuleN, Neural LP, DRUM, GraIL and RED-GNN on WN18RR (V1), FB15k-237 (V1) and NELL-995 (V1). Both training and inference are very efficient in RuleN. Neural LP and DRUM have similar cost but are more expensive than RED-GNN by using the full adjacency matrix. For GraIL, both training and inference are very expensive since they require bidirectional sampling to extract the subgraph and then compute for each triple. Overall, RED-GNN is more efficient than the differentiable methods Neural LP, DRUM and GraIL.

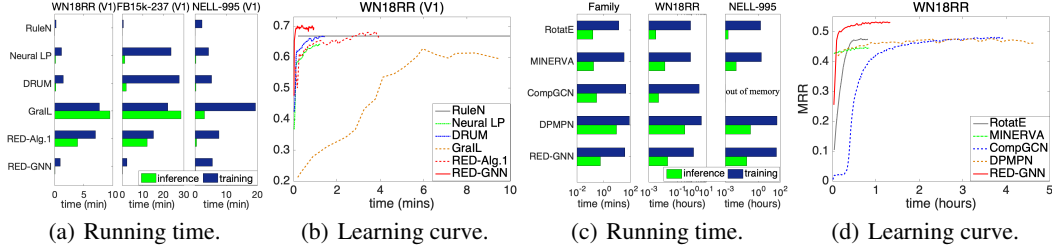


Figure 2: Running time analysis and learning curve on WN18RR (V1) and WN18RR.

For reasoning on incomplete KG, we compare RotatE, MINERVA, CompGCN, DPMPN and RED-GNN on Family, WN18RR and NELL-995. Due to the simple training framework on triples, RotatE is the most efficient method. MINERVA is more efficient than GNN-based methods since the sampled paths have simpler structures. CompGCN, with fewer layers, has similar cost with RED-GNN as its computation is on the whole graph. For DPMPN, the pruning is expensive and it has two GNNs working together, thus it is more expensive than RED-GNN. Since GraIL is hundreds of times more expensive than RED-GNN, it is intractable on the larger KGs in this setting.

5.4 Ablation study

Interpretation. We visualize exemplar learned r-digraphs by RED-GNN with $L = 3$ on the Family and UMLS datasets. Given the triple (e_q, r_q, e_a) , we remove the edges in $\mathcal{G}_{e_q, e_a|L}$ whose attention weights are less than 0.5, and extract the remaining parts. Fig.3(a) shows one triple that DRUM fails. As shown, inferring id-1482 as the son of id-1480 requires the knowledge that id-1480 is the only brother of the uncle id-1432 from the local structure. Fig.3(b) and 3(c) show two examples with the same e_q and e_a , sharing the same digraph $\mathcal{G}_{e_q, e_a|L}$. First, RED-GNN can learn distinctive structures for different query relations, which caters to Theorem 4.3. Second, RED-GNN can learn similar structures for a certain relation, such as *Complicates*, verifying the transferability across triples regardless of the identity of entities. The examples in Fig.3 demonstrate that RED-GNN is interpretable. We provide more examples and the visualization algorithm in Appendix C.

Variants of RED-GNN. Tab.3 shows the performance of different variants. First, we study the impact of removing r_q in attention (denoted as Attn-w.o.- r_q). Specifically, we remove $\mathbf{h}_{r_q}^\ell$ from the attention weight $\alpha_{e_s, r, r_q}^\ell$ in (4) and change the scoring function to $\mathbf{w}^\top (\mathbf{h}_{e_a}^L(e_q, r_q) \oplus \mathbf{h}_{r_q})$, with $\mathbf{w} \in \mathbb{R}^{2d}$. Since the $\alpha_{e_s, r, r_q}^\ell$ aims to figure out the important edges in $\mathcal{G}_{e_q, e_a|L}$, the learned structure will be less informative without the control of the query relation r_q , thus has poor performance.

Second, we replace Alg.2 in RED-GNN with the simple r-digraph encoding by Alg.1 (denoted as RED-Alg.1). Due to the efficiency issue, the loss function (5), computing the scores over $|\mathcal{V}|$ triples for each sample, cannot be used. Hence, we use the margin ranking loss with 1 negative sample as in GraIL [29]. As in Tab.3, the performance of RED-Alg.1 is weak than RED-GNN since the multi-class log loss is better than loss functions with negative sampling [17, 24]. RED-Alg.1 still outperforms GraIL in Tab. 1 since the r-digraphs are better structures for reasoning. The running time of RED-Alg.1 is in Fig.2(a) and 2(b). Alg.1 is much more expensive than Alg.2 but is cheaper than GraIL since GraIL needs the Dijkstra algorithm to label the entities.

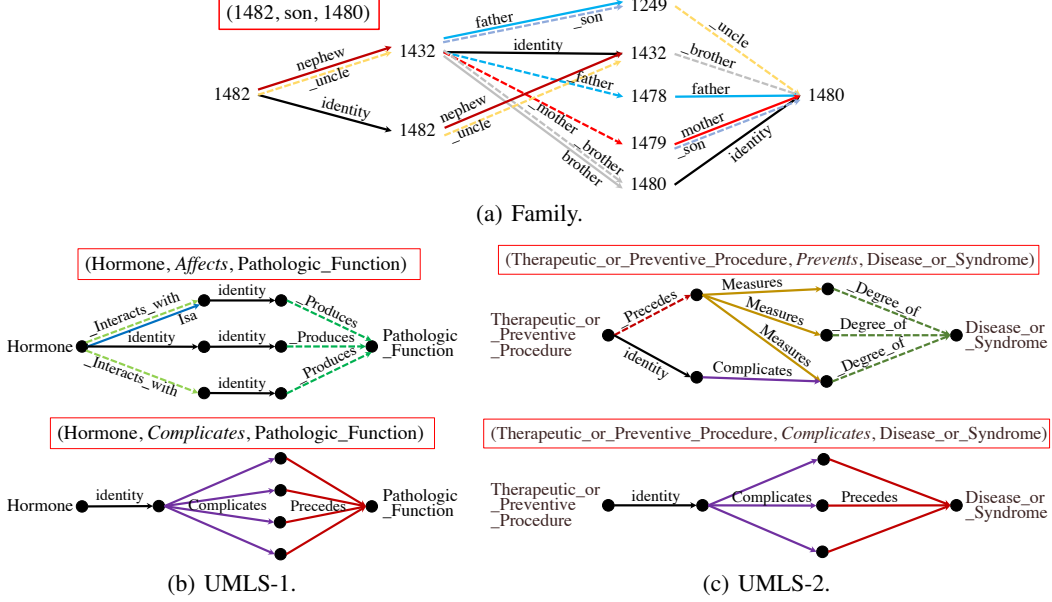


Figure 3: Visualization of the learned structures. Dashed lines mean inverse relations. The query triples are indicated by the red rectangles. Due to space limitation, entities in UMLS dataset are shown as black circles (best viewed in color).

Depth of models. In Fig.4, we show the influence of testing MRR with different layers or steps L in the left y -axis. The coverage (in %) of testing triples (e_q, r_q, e_a) where e_a is visible from e_q in L steps, i.e., $e_a \in \mathcal{V}_{e_q}^L$, is shown in the right y -axis. Intuitively, when L increases, more triples will be covered, paths or subgraphs between e_q and e_a then contain richer information, but will be harder to learn. As shown, the performance of DRUM, Neural LP and MINERVA decreases for $L \geq 4$. CompGCN runs out of memory when $L > 3$ and it is also hard to capture complex structures with $L = 3$. When L is too small, e.g., $L \leq 2$, RED-GNN has poor performance mainly due to limited information encoded in such small r-digraphs. RED-GNN achieves the best performance for $L \geq 3$ where the r-digraphs can contain richer information and the important information for reasoning can be effectively learned by (3). Since the computation cost significantly increases with L , we tune $L \in \{3, 4, 5\}$ to balance the efficiency and effectiveness in practice.

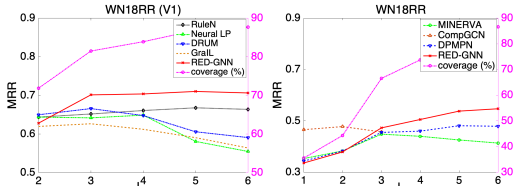


Figure 4: The MRR performance with different L and coverage of triples within L steps.

Table 4: The per-distance evaluation for MRR on WN18RR v.s. the length of shortest path.

distance	1	2	3	4	5	>5
ratios (%)	34.9	9.3	21.5	7.5	8.9	17.9
CompGCN	.993	.327	.337	.062	.061	.016
DPMPN	.982	.381	.333	.102	.057	.001
RED-GNN	.993	.563	.536	.186	.089	.005

Per-distance performance. Note that given a r-digraph with L layers, the information between two nodes that are not reachable with L hops cannot be propagated by Alg.2. This may raise a concern about the predicting ability of RED-GNN, especially for triples not reachable in L steps. We demonstrate this is not a problem here. Specifically, given a triple (e_q, r_q, e_a) , we compute the shortest distance from e_q to e_a . Then, the MRR performance is grouped in different distances. We compare CompGCN ($L = 2$), DPMPN ($L = 5$) and RED-GNN ($L = 5$) in Tab.4. All the models have worse performance on triples with larger distance and cannot well model the triples that are far away. RED-GNN has the best per-distance performance within distance 5.

6 Conclusion

In this paper, we introduce a novel relational structure, i.e., r-digraph, as a generalized structure of relational paths for KG reasoning. Individually computing on each r-digraph is expensive for

the reasoning task $(e_q, r_q, ?)$. Hence, inspired by solving overlapping sub-problems by dynamic programming, we propose RED-GNN as a variant of GNN, to efficiently construct and effectively learn the r-digraph. We show that RED-GNN achieves the state-of-the-art performance in both KG with unseen entities and incomplete KG benchmarks. The training and inference of RED-GNN are very efficient compared with the other GNN-based baselines. Besides, interpretable structures for reasoning can be learned by RED-GNN. One limitation of this work is that it will be slow and requires more memory resources for even larger KGs such as ogbl-biokg and ogbl-wikikg2 [12]. In future work, we can leverage the pruning technique in [38] or distributed programming in [5] to make RED-GNN work on KG with extremely large scale.

References

- [1] P. Battaglia, J. B. Hamrick, V. Bapst, A. Sanchez-Gonzalez, V. Zambaldi, M. Malinowski, et al. Relational inductive biases, deep learning, and graph networks. Technical report, arXiv:1806.01261, 2018.
- [2] Di Battista, G, P. Eades, R. Tamassia, and I. Tollis. *Graph drawing: algorithms for the visualization of graphs*. Prentice Hall PTR, 1998.
- [3] A. Bordes, N. Usunier, A. Garcia-Duran, J. Weston, and O. Yakhnenko. Translating embeddings for modeling multi-relational data. In *NeurIPS*, pages 2787–2795, 2013.
- [4] X. Chen, S. Jia, and Y. Xiang. A review: Knowledge reasoning over knowledge graph. *Expert Systems with Applications*, 141:112948, 2020.
- [5] W. W Cohen, H. Sun, R A. Hofer, and M. Sieglar. Scalable neural methods for reasoning with a symbolic knowledge base. In *ICLR*, 2019.
- [6] R. Das, S. Dhuliawala, M. Zaheer, L. Vilnis, I. Durugkar, A. Krishnamurthy, A. Smola, and A. McCallum. Go for a walk and arrive at the answer: Reasoning over paths in knowledge bases using reinforcement learning. In *ICLR*, 2017.
- [7] T. Dettmers, P. Minervini, P. Stenetorp, and S. Riedel. Convolutional 2D knowledge graph embeddings. In *AAAI*, 2017.
- [8] J. Gilmer, S. S Schoenholz, P. F Riley, O. Vinyals, and G. E Dahl. Neural message passing for quantum chemistry. In *ICML*, pages 1263–1272, 2017.
- [9] W. Hamilton, Z. Ying, and J. Leskovec. Inductive representation learning on large graphs. In *NeurIPS*, pages 1024–1034, 2017.
- [10] Z. Han, P. Chen, Y. Ma, and V. Tresp. Explainable subgraph reasoning for fore-casting on temporal knowledge graphs. In *ICLR*, 2021.
- [11] K. Hornik. Approximation capabilities of multilayer feedforward networks. *Neural networks*, 4(2):251–257, 1991.
- [12] W. Hu, M. Fey, M. Zitnik, Y. Dong, H. Ren, B. Liu, M. Catasta, and J. Leskovec. Open graph benchmark: Datasets for machine learning on graphs. In *NeurIPS*, 2020.
- [13] S. Ji, S. Pan, E. Cambria, P. Marttinen, and P. Yu. A survey on knowledge graphs: Representation, acquisition and applications. Technical report, arXiv:2002.00388, 2020.
- [14] D. P Kingma and J. Ba. Adam: A method for stochastic optimization. Technical report, arXiv:1412.6980, 2014.
- [15] T. Kipf and M. Welling. Semi-supervised classification with graph convolutional networks. In *ICLR*, 2016.
- [16] S. Kok and P. Domingos. Statistical predicate invention. In *ICML*, pages 433–440, 2007.
- [17] T. Lacroix, N. Usunier, and G. Obozinski. Canonical tensor decomposition for knowledge base completion. In *ICML*, pages 2863–2872, 2018.
- [18] N. Lao and W. W Cohen. Relational retrieval using a combination of path-constrained random walks. *Machine learning*, 81(1):53–67, 2010.
- [19] N. Lao, T. Mitchell, and W. Cohen. Random walk inference and learning in a large scale knowledge base. In *EMNLP*, pages 529–539, 2011.
- [20] C. Meilicke, M. Fink, Y. Wang, D. Ruffinelli, R. Gemulla, and H. Stuckenschmidt. Fine-grained evaluation of rule-and embedding-based systems for knowledge graph completion. In *ISWC*, pages 3–20. Springer, 2018.
- [21] M. Niepert. Discriminative gaifman models. In *NIPS*, volume 29, pages 3405–3413, 2016.
- [22] A. Paszke, S. Gross, S. Chintala, G. Chanan, E. Yang, Z. DeVito, Z. Lin, A. Desmaison, L. Antiga, and A. Lerer. Automatic differentiation in PyTorch. In *ICLR*, 2017.
- [23] M. Qu, J. Chen, L. Xhonneux, Y. Bengio, and J. Tang. Rnnlogic: Learning logic rules for reasoning on knowledge graphs. In *ICLR*, 2021.
- [24] D. Ruffinelli, S. Broscheit, and R. Gemulla. You can teach an old dog new tricks! on training knowledge graph embeddings. In *ICLR*, 2020.

- [25] A. Sadeghian, M. Armandpour, P. Ding, and D Wang. Drum: End-to-end differentiable rule mining on knowledge graphs. In *NeurIPS*, pages 15347–15357, 2019.
- [26] M. Schlichtkrull, T. N Kipf, P. Bloem, Rianne Van D., I. Titov, and M. Welling. Modeling relational data with graph convolutional networks. In *ESWC*, pages 593–607. Springer, 2018.
- [27] Y. Shen, J. Chen, Y. Huang, P. Guo, and J. Gao. M-walk: Learning to walk over graphs using monte carlo tree search. In *NeurIPS*, 2018.
- [28] Z. Sun, Z. Deng, J. Nie, and J. Tang. RotatE: Knowledge graph embedding by relational rotation in complex space. In *ICLR*, 2019.
- [29] K. K Teru, E. Denis, and W. Hamilton. Inductive relation prediction by subgraph reasoning. In *ICML*, 2020.
- [30] K. Toutanova and D. Chen. Observed versus latent features for knowledge base and text inference. In *PWCVSMC*, pages 57–66, 2015.
- [31] T. Trouillon, C. R Dance, É. Gaussier, J. Welbl, S. Riedel, and G. Bouchard. Knowledge graph completion via complex tensor factorization. *JMLR*, 18(1):4735–4772, 2017.
- [32] S. Vashishth, S. Sanyal, V. Nitin, and P. Talukdar. Composition-based multi-relational graph convolutional networks. In *ICLR*, 2019.
- [33] P. Veličković, G. Cucurull, A. Casanova, A. Romero, P. Lio, and Y. Bengio. Graph attention networks. In *ICLR*, 2017.
- [34] H. Wang, H. Ren, and J. Leskovec. Entity context and relational paths for knowledge graph completion. Technical report, arXiv:2002.06757, 2020.
- [35] Q. Wang, Z. Mao, B. Wang, and L. Guo. Knowledge graph embedding: A survey of approaches and applications. *TKDE*, 29(12):2724–2743, 2017.
- [36] W. Xiong, T. Hoang, and W. Wang. Deeppath: A reinforcement learning method for knowledge graph reasoning. In *EMNLP*, pages 564–573, 2017.
- [37] K. Xu, W. Hu, J. Leskovec, and S. Jegelka. How powerful are graph neural networks? In *ICLR*, 2018.
- [38] X. Xu, W. Feng, Y. Jiang, X. Xie, Z. Sun, and Z. Deng. Dynamically pruned message passing networks for large-scale knowledge graph reasoning. In *ICLR*, 2019.
- [39] F. Yang, Z. Yang, and W. Cohen. Differentiable learning of logical rules for knowledge base reasoning. In *NeurIPS*, pages 2319–2328, 2017.
- [40] S. Yun, M. Jeong, R. Kim, J. Kang, and H. J Kim. Graph transformer networks. *NeurIPS*, 32:11983–11993, 2019.
- [41] S. Zhang, Y. Tay, L. Yao, and Q. Liu. Quaternion knowledge graph embeddings. In *NeurIPS*, 2019.
- [42] H. Zhao, Q. Yao, J. Li, Y. Song, and K. L. Lee. Meta-graph based recommendation fusion over heterogeneous information networks. In *SIGKDD*, pages 635–644, 2017.

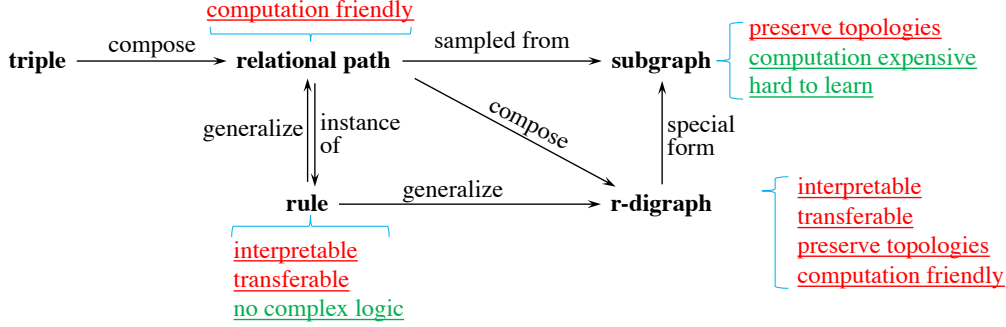


Figure 5: Graphical view of the position of the r-digraph.

To begin with, we first illustrate again the position of r-digraph in Fig.5. Since **relational paths** are composed of **triples**, they can naturally be more informative than the **triples**. **Rules** are the generalized form of **relational paths** and **relational paths** serve as the instance of **rules**. The benefits of **rules** are that they are interpretable, transferable to unseen entities and computation friendly with the sequential structure. However, they cannot model complex structural information that lies in the topological structures.

The idea of upgrading path learning to subgraph learning is similar as triple learning to path learning as **relational paths** are sampled from local **subgraphs**. **Subgraphs** can preserve more topology information but they are computationally expensive with the complex structures, and it is hard to learn the essential information in the mixed edges. This motivates us to design **r-digraph** that is a special form of **subgraph**, is composed by the **relational paths** and serves as a generalized form of **rules**. This makes it interpretable and transferable as **rules**, computation friendly as **relational paths**, and able to model complex logics.

A Experiment materials

A.1 Implementation details

Efficient sampling. Given the augmented triples \mathcal{F} , we introduce how to efficiently collect $\hat{\mathcal{E}}_{e_q}^\ell$ and $\mathcal{V}_{e_q}^\ell$ in step 3 in Algorithm 2. The implementation borrows the idea of using the sparse matrix for representing symbols in KG [5]. First, we build a sparse subject-fact matrix $\mathbf{M} \in \mathbb{R}^{|\mathcal{V}| \times |\mathcal{F}|}$ and $M_{ij} = 1$ if the i -th entity is the subject entity of the j -th triple. We then form a sparse matrix $\mathbf{E}_{e_q}^\ell$ whose rows are one-hot representations for entities in $\mathcal{V}_{e_q}^{\ell-1}$. Next, we can use the sparse matrix multiplication $\mathbf{E}_{e_q}^\ell \times \mathbf{M}$ to get the indices of triples in \mathcal{F} . Then the triples obtained by these indices are used to form $\hat{\mathcal{E}}_{e_q}^\ell$. $\mathcal{V}_{e_q}^\ell$ is updated by the collecting the set of tail entities in $\hat{\mathcal{E}}_{e_q}^\ell$. This procedure can be efficient since both $\mathbf{E}_{e_q}^\ell$ and \mathbf{M} are sparse matrices.

Mini-batch computation. For different query triples (e_q, r_q, e_a) in a mini-batch, they may correspond to different queries $(e_q, r_q, ?)$. Since the GNN in Section 4.2 is query-dependent, we should independently learn on each triple. For efficiency consideration, we add an index for each triple as (id, e_q, r_q, e_a) in the mini-batch so that different r-digraphs and triples can be constructed and computed in parallel, and entities corresponding to different queries will not be in conflict. Besides, adding an index id can also leverage the efficient sampling method in previous paragraph by preserving the id for each matrix $\mathbf{E}_{e_q}^\ell$ with the shared \mathbf{M} .

A.2 Setup for KG with unseen entities

Hyper-parameters. For RED-GNN, we tune the learning rate in $[10^{-4}, 10^{-2}]$, weight decay in $[10^{-5}, 10^{-2}]$, dropout rate in $[0, 0.3]$, batch size in $\{5, 10, 20, 50, 100\}$, dimension d in $\{32, 48, 64, 96\}$, d_α for attention in $\{3, 5\}$, layer L in $\{3, 4, 5\}$, and activation function δ in $\{\text{identity}, \text{tanh}, \text{ReLU}\}$. Adam [14] is used as the optimizer. The best hyper-parameter settings are selected by the MRR

metric on \mathcal{T}_{val} with maximum training epochs of 50. For RuleN, we use the code² with default setting. For Neural LP³, and DRUM⁴ we tune the learning rate in $[10^{-4}, 10^{-2}]$, dropout rate in $[0, 0.3]$, batch size in batch size in $\{20, 50, 100\}$, dimension d in $\{64, 128\}$, layer L of RNN in $\{1, 2\}$, and number of steps in $\{2, 3, 4, 5\}$. For GraIL⁵, we tune the learning rate in $[10^{-5}, 10^{-2}]$, weight decay in $[10^{-6}, 10^{-3}]$, batch size in $\{8, 16, 32\}$, dropout rate in $[0, 0.4]$, edge_dropout rate in $[0, 0.6]$, GNN aggregator among $\{\text{sum}, \text{MLP}, \text{GRU}\}$ and hop numbers among $\{2, 3, 4\}$. The training epochs are all set as 50.

Tie policy. In evaluation, the tie policy is important. Specifically, when there are triples with the same rank, choosing the largest rank and smallest rank in the tie will lead to rather different results. Considering that we give the same score 0 for triples where $\mathcal{G}_{e_q, e_a|L} = \emptyset$, there will be a concern of the tie policy. Hence, we use the average rank among the triples in tie as suggested by the paper “Knowledge Graph Embedding for Link Prediction: A Comparative Analysis”.

Benchmarks. We use the 12 groups of benchmark dataset in [29] in the URL <https://github.com/kkteru/grail/tree/master/data>. The detailed statistics are summarized in Tab.5.

Table 5: Statistics of the benchmarks with unseen entities (inductive). “fact” denotes the number of triples used as graph, and “pred” means the triples used for reasoning.

datasets		WN18RR				FB15k-237				NELL-995			
		ent	rel	fact	pred	ent	rel	fact	pred	ent	rel	fact	pred
v1	train	2746	9	5410	1268	1594	180	4245	981	3102	14	4687	853
	test	922		1618	373			1993	411			833	201
v2	train	6954	10	15262	3706	1608	200	9739	2346	2563	88	8219	1890
	test	5084		4011	852			4145	947			4586	935
v3	train	12078	11	25901	6249	3668	215	17986	4408	4647	142	16393	3724
	test	5084		6327	1140			7406	1731			8048	1620
v4	train	3861	9	7940	1902	4707	219	27203	6713	2092	76	7546	1743
	test	7084		12334	2823			11714	2840			7073	1447

Results. The full results with MRR, Hit@1 and Hit@10 metrics are shown in Tab.6.

A.3 Setup for incomplete KG

Hyper-parameters. The tuning ranges of hyper-parameters of RED-GNN are the same as those in Appendix A.2. For RotatE and QuatE, we tune the dimensions in $\{100, 200, 500, 1000\}$, batch_size in $\{256, 512, 1024, 2048\}$, weight decay in $[10^{-5}, 10^{-2}]$, number of negative samples in $\{64, 128, 256, 512, 1024\}$, with training iterations of 100000. For MINERVA, Neural LP, DRUM and DPMPN we use their default setting as the figures are provided. For CompGCN, we choose the scoring function as ConvE the composition operator as correlation as suggested in their paper [32]. and tune the learning rate in $[10^{-4}, 10^{-2}]$, layer in $\{1, 2, 3\}$ and dropout rate in $[0, 0.3]$ with training epochs of 300.

Benchmarks. We provide the statistics of entities, relations and split of triples in Tab.7. The data split is same as those in the literature [39, 25] for Family, UMLS, WN18RR and FB15k-237 in the public link <https://github.com/alisdadeghian/DRUM/tree/master/datasets>. For NELL-995, we use the version in <https://github.com/thunlp/OpenKE/tree/OpenKE-PyTorch/benchmarks/NELL-995>.

A.4 Optimal hyper-parameters

We summarize the optimal hyper-parameters for reproducing the results of RED-GNN on each benchmarks in Tab.8.

²<https://github.com/kkteru/grail/tree/master/ruleN>

³<https://github.com/fanyangxyz/Neural-LP>

⁴<https://github.com/alisdadeghian/DRUM>

⁵<https://github.com/kkteru/grail/>

Table 6: Results on KG with unseen entities. Best performance is indicated by the bold face numbers.

		WN18RR				FB15k-237				NELL-995			
		V1	V2	V3	V4	V1	V2	V3	V4	V1	V2	V3	V4
MRR	RuleN	.668	.645	.368	.624	.363	.433	.439	.429	.615	.385	.381	.333
	Neural LP	.649	.635	.361	.628	.325	.389	.400	.396	.610	.361	.367	.261
	DRUM	.666	.646	.380	.627	.333	.395	.402	.410	.628	.365	.375	.273
	GraIL	.627	.625	.323	.553	.279	.276	.251	.227	.481	.297	.322	.262
	RED-GNN	.701	.690	.427	.651	.369	.469	.445	.442	.637	.419	.436	.363
Hit@1	RuleN	63.5	61.1	34.7	59.2	30.9	34.7	34.5	33.8	54.5	30.4	30.3	24.8
	Neural LP	59.2	57.5	30.4	58.3	24.3	28.6	30.9	28.9	50.0	24.9	26.7	13.7
	DRUM	61.3	59.5	33.0	58.6	24.7	28.4	30.8	30.9	50.0	27.1	26.2	16.3
	GraIL	55.4	54.2	27.8	44.3	20.5	20.2	16.5	14.3	42.5	19.9	22.4	15.3
	RED-GNN	65.3	63.3	36.8	60.6	30.2	38.1	35.1	34.0	52.5	31.9	34.5	25.9
Hit@10	RuleN	73.0	69.4	40.7	68.1	44.6	59.9	60.0	60.5	76.0	51.4	53.1	48.4
	Neural LP	77.2	74.9	47.6	70.6	46.8	58.6	57.1	59.3	87.1	56.4	57.6	53.9
	DRUM	77.7	74.7	47.7	70.2	47.4	59.5	57.1	59.3	87.3	54.0	57.7	53.1
	GraIL	76.0	77.6	40.9	68.7	42.9	42.4	42.4	38.9	56.5	49.6	51.8	50.6
	RED-GNN	79.9	78.0	52.4	72.1	48.3	62.9	60.3	62.1	86.6	60.1	59.4	55.6

Table 7: Statistics of benchmarks for incomplete KG benchmarks (transductive). Note that NELL-995* is different as the version in [6] since the training triples contains valid and test triples there.

	$ \mathcal{V} $	$ \mathcal{R} $	$ \mathcal{F} $	$ \mathcal{F}_{\text{val}} $	$ \mathcal{F}_{\text{test}} $
Family	3,007	12	23,483	2,038	2,835
UMLS	135	46	5,327	569	633
WN18RR	40,943	11	86,835	3,034	3,134
FB15k-237	14,541	237	272,115	17,535	20,466
NELL-995*	74,536	200	149,678	543	2,818

Table 8: Hyper-parameter settings on the different benchmarks.

benchmarks	learning rate	weight decay	dropout	batch size	d	d_α	L	δ
WN18RR (V1)	0.005	0.0002	0.21	100	64	5	5	ReLU
WN18RR (V2)	0.0016	0.0004	0.02	20	48	3	5	ReLU
WN18RR (V3)	0.0014	0.000034	0.28	20	64	5	5	tanh
WN18RR (V4)	0.006	0.00013	0.11	10	32	5	5	ReLU
FB15k-237 (V1)	0.0092	0.0003	0.23	20	32	5	3	ReLU
FB15k-237 (V2)	0.0077	0.0002	0.3	10	48	5	3	ReLU
FB15k-237 (V3)	0.0006	0.000023	0.27	20	48	3	3	ReLU
FB15k-237 (V4)	0.0052	0.000018	0.07	20	48	5	5	idd
NELL-995 (V1)	0.0021	0.00019	0.25	10	48	5	5	relu
NELL-995 (V2)	0.0075	0.00066	0.29	100	48	5	3	ReLU
NELL-995 (V3)	0.0008	0.0004	0.06	10	16	3	3	ReLU
NELL-995 (V4)	0.0005	0.0004	0.15	20	16	5	5	tanh
Family	0.0036	0.000017	0.29	20	48	3	5	ReLU
UMLS	0.0012	0.00014	0.12	10	64	5	5	tanh
WN18RR	0.0003	0.00014	0.02	50	64	5	5	idd
FB15k-237	0.0009	0.00008	0.04	5	48	5	4	ReLU
NELL	0.0011	0.000089	0.26	5	48	5	5	ReLU

A.5 Running time

We have shown the learning curves on WN18RR and WN18RR (V1) in Sect. 5. In this part, we provide the learning curves on Family, UMLS, FB15k-237, FB15k-237 (V1) and NELL-995 (V1).

in Fig.6. Since the results of FB15k-237 are directly copied from the results in the baseline papers, we simply provide the learning curve of RED-GNN here. For RuleN, the learning curve is not available. For GraIL and RED-Alg.1, the evaluation is costly, thus the learning curves are not provided. Instead, we plot RuleN, GraIL and RED-Alg.1 as lines with their training time as starting point. These figures have similar observation as those in Sect. 5.

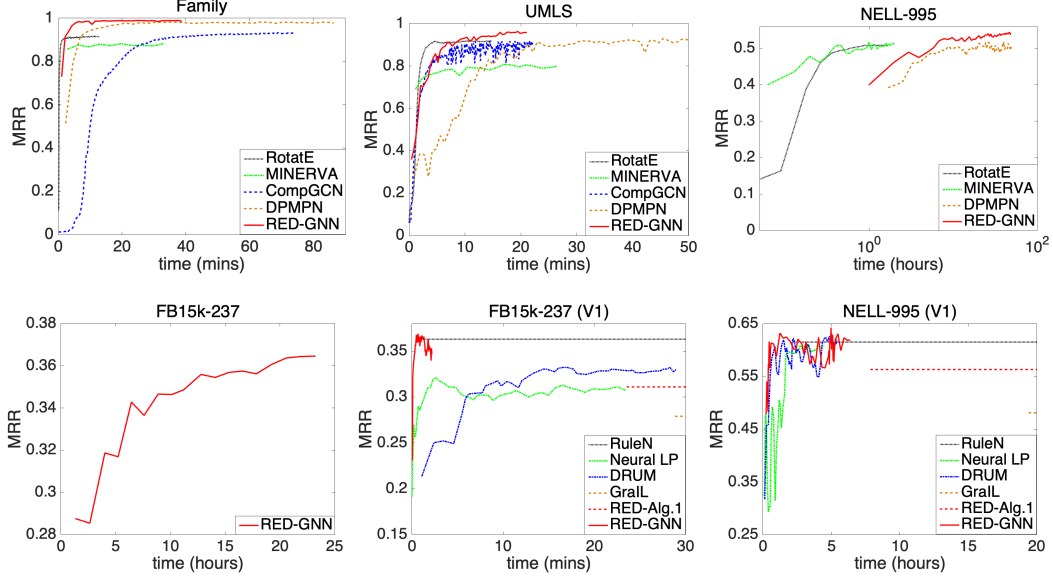


Figure 6: Learning curves.

A.6 Influence of depth

In this part, we provide the influence of depth on the Family, UMLS, FB15k-237 (V1) and NELL-995 (V1) benchmarks in Fig.7.

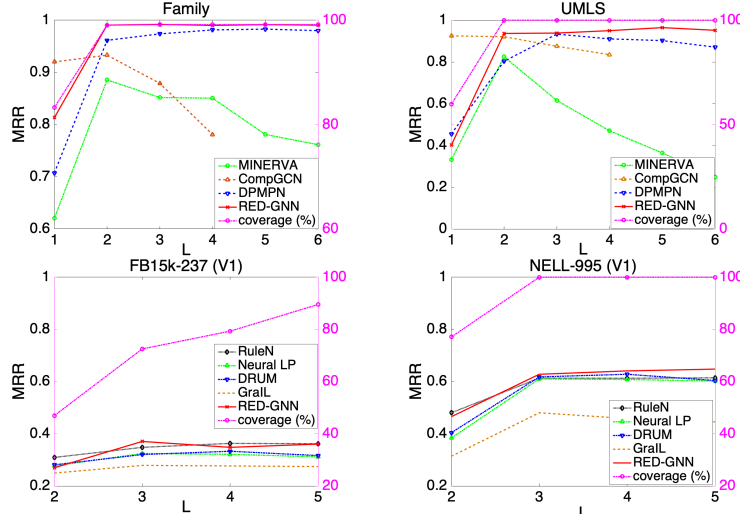


Figure 7: The MRR performance with different L and coverage of triples within L steps.

B Inference complexity

In this part, we explain how the inference complexity is computed. When reasoning on the query $(e_q, r_q, ?)$, we need to evaluate $|\mathcal{V}|$ triples with the different answer entity $e \in \mathcal{V}$. We assume the average degree as \bar{D} and average number of edges in each layer of r-digraph as \bar{E} .

- Algorithm 1. For construction, the main cost comes from extracting the neighbors $\mathcal{E}_{e_q}^\ell$ and $\mathcal{V}_{e_q}^\ell$ of e_q . In general, the cost is \bar{D}^L for sampling the L -hop neighbors. The extreme case is that the KG is a complete graph and the cost is $(|\mathcal{F}|(L-1))$. Thus, the cost for construction is $O(\min(\bar{D}^L, |\mathcal{F}|L))$. For encoding, the cost is $O(d\bar{E}L)$ for the message passing steps. Thus, the total cost is $O(\min(\bar{D}^L, |\mathcal{F}|L) + d\bar{E}L)$.
- Algorithm 2. Since the full computation is conducted on $\mathcal{E}_{e_q}^\ell$ and $\mathcal{V}_{e_q}^\ell$, thus the cost is the number of edges times the dimension d , i.e. $O(\min(\bar{D}^L, |\mathcal{F}|L) \cdot d)$. Since $d \ll |\mathcal{V}|$, the complexity is strongly reduced compared with Algorithm 1.

We also show the complexity of the other GNN-based methods.

- CompGCN. All the representations are aggregated in one pass with cost $O(|\mathcal{F}|dL)$. Then the scores for all the entities are computed with cost $O(|\mathcal{V}|d)$, thus the total cost is $O(|\mathcal{F}|dL + |\mathcal{V}|d)$.
- DPMPN. Denote the dimension and layer in the non-attentive GNN as d_1, L_1 , the maximum degree of the sampled edges in the pruning procedure as \bar{D} . Then, the main cost comes from the non-attentive GNN with cost $O(|\mathcal{F}|d_1L_1)$. The cost on sampled subgraph is $O(\bar{D}^Ld)$. Thus, the total computation cost is $O(|\mathcal{F}|d_1L_1 + \bar{D}^Ld)$.
- GraIL. The complexity in constructing the enclosing subgraph is $O(\bar{E} \log(V))$ with \bar{E} edges and \bar{V} entities. The computation cost of the GNN module is $O(\bar{E}dL)$. Since each triple requires a construction and computation, the overall cost is $O(|\mathcal{V}|(\bar{E} \log \bar{V} + \bar{E}dL))$.

C Visualization

We summarize the steps for visualizing the r-digraph learned between entities in Algorithm 3. The key point is to backtrack the neighborhood edges of e_a that has attention weight larger than a pre-defined threshold $\theta > 0$, i.e., step 3-6. The remaining structures $\mathcal{G}_{e_q, e_a|L}(\theta)$ are returned as the structure selected by the attention weights.

Algorithm 3 Visualization.

Require: entities \mathcal{V} , triples \mathcal{F} , query triple (e_q, r_q, e_a) , depth L , parameters Θ , threshold θ .

- 1: Run Alg.2 to obtain the attention weight $\alpha_{e_s, r, r_q}^\ell, \ell = 1 \dots L$ on the edges in each layer.
 - 2: Initialize $\mathcal{V}_{e_q, e_a|L}^L(\theta) = \{e_a\}$.
 - 3: **for** $\ell = L, L-1 \dots 1$ **do**
 - 4: collect the edges $\mathcal{E}_{e_q, e_a|L}^\ell(\theta) = \{(e_s, r, e_o) | e_o \in \mathcal{V}_{e_q, e_a|L}^L, \alpha_{e_s, r, r_q}^\ell \geq \theta\}$.
 - 5: collect the entities $\mathcal{V}_{e_q, e_a|L}^{\ell-1}(\theta) = \{e_s | (e_s, r, e_o) \in \mathcal{E}_{e_q, e_a|L}^\ell(\theta)\}$.
 - 6: **end for**
 - 7: **return** $\mathcal{G}_{e_q, e_a|L}(\theta) = \mathcal{E}_{e_q, e_a|L}^1(\theta) \otimes \mathcal{E}_{e_q, e_a|L}^2(\theta) \dots \otimes \mathcal{E}_{e_q, e_a|L}^L(\theta)$.
-

We provide some additional visualized results on Family and UMLS datasets in Fig. 8 and Fig. 9, respectively. As shown, there are consistent and semantically friendly patterns across different query triples.

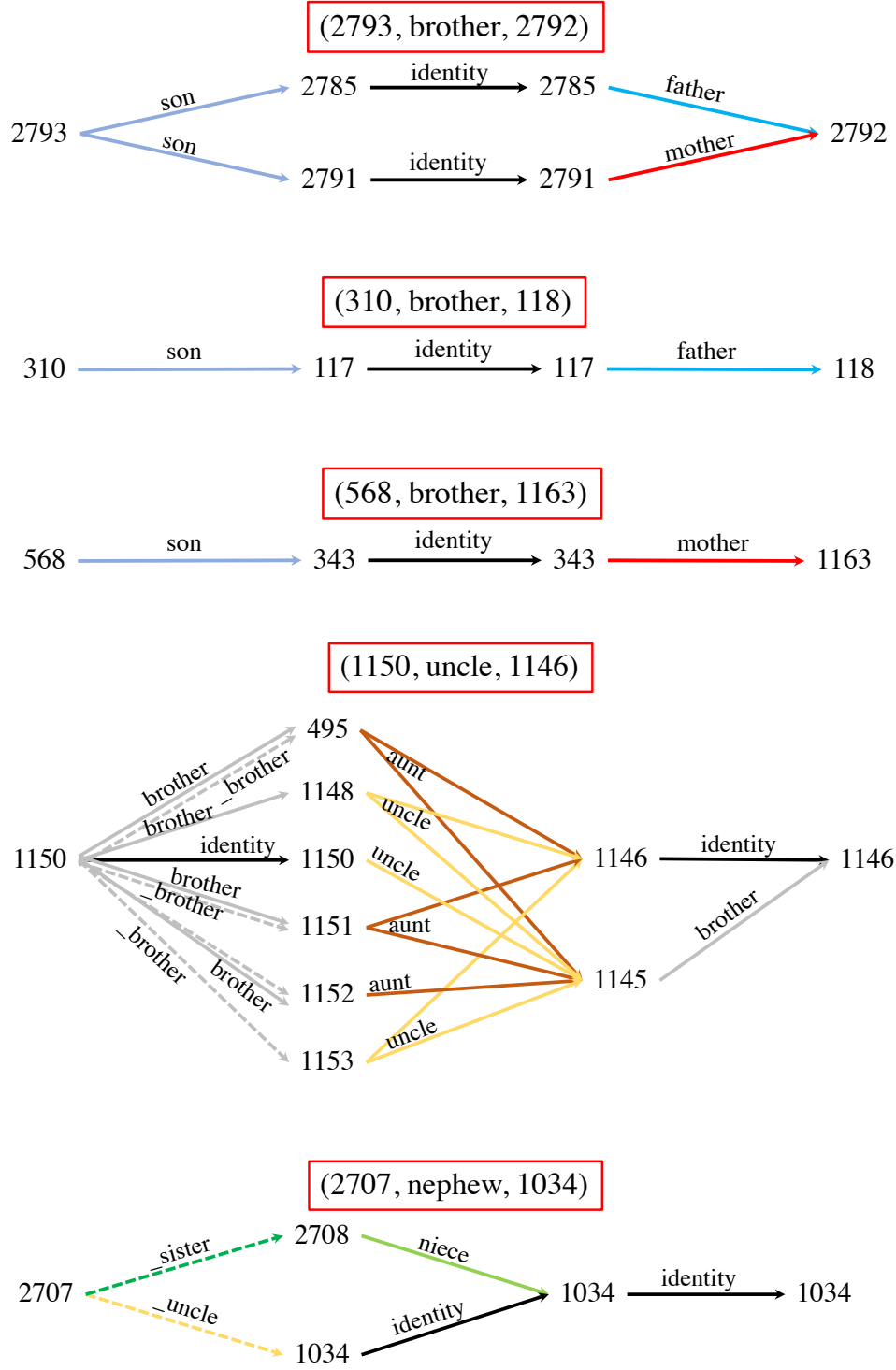
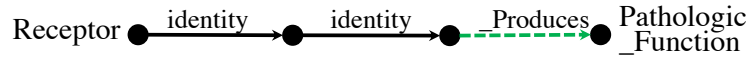
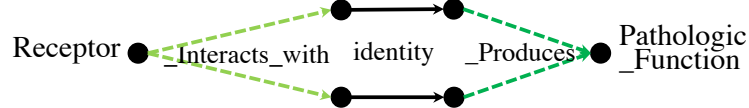


Figure 8: Visualization of the learned structure on Family.

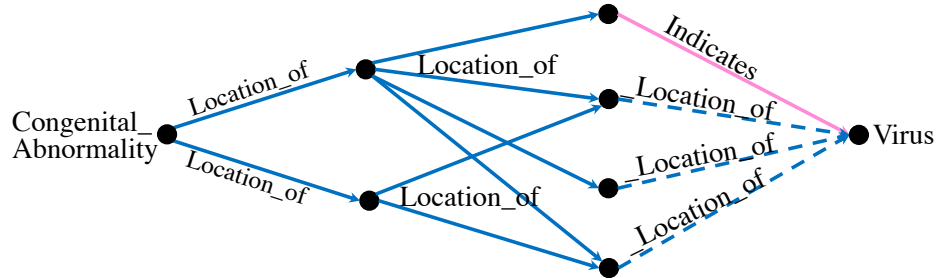
(Receptor, Causes, Pathologic_Function)



(Receptor, Affects, Pathologic_Function)



(Congenital_Abnormality, Location_of, Virus)



(Therapeutic_or_Preventive_Procedure, Isa, Activity)

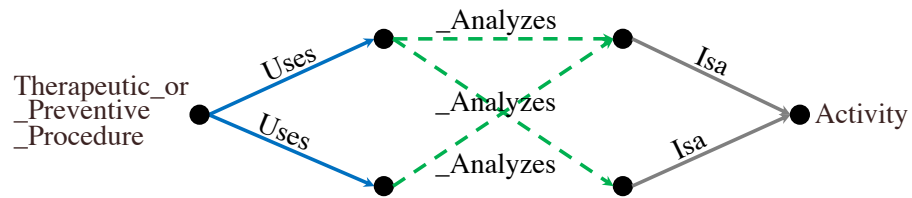


Figure 9: Visualization of the learned structure on UMLS.

D Problem analysis on GraIL

As mentioned in the main text, efficiency is the preliminary issue of GraIL [29]. In this part, we mainly analyze it in terms of effectiveness.

D.1 Enclosing subgraph v.s. r-digraph

When constructing the enclosing subgraph, the bidirectional information between e_q and e_a is preserved. In other words, it contains all the relational paths from e_q to e_a and all the paths from e_a to e_q . This is the key difference between enclosing subgraph and r-digraph. In this view, the limitations of the enclosing subgraph can be summarized as follows.

- Since the entire subgraph is extracted, there is no much different between different entities in the enclosing subgraph. Thus, it requires a distance labeling to indicate how far away an entity is to the query entity and answer entity. In the r-digraph, the distance can be indicated by the layer and update frequency of different entities. The entity in the first layer is the query entity and the entity in the last layer is the answer entity.
- The information flow, i.e. the order of relations, inside the enclosing subgraph is mixed, making it hard to learn the dependency among relations. This is important since the order of relations reflects the logical patterns, e.g. the difference between *brother* \wedge *mother* \rightarrow *uncle* and *mother* \wedge *brother* \rightarrow *aunt*. In GraIL, there is no explicit direction for the relation to be ordered. They can only be implicitly captured if the attention weights are perfectly learned.

The enclosing subgraph, even though contains more edges than the r-digraph, does not show valuable inductive bias for KG reasoning.

D.2 Non-interpretable

In GraIL, the final scoring is on a graph-level representation

$$h_{\mathcal{G}(e_q, r_q, e_a)}^L = \frac{1}{|\mathcal{V}_{e_q, e_a}|} \sum_{i \in \mathcal{V}_{e_q, e_a}} h_i^L,$$

where \mathcal{V}_{e_q, e_a} is the entities in the enclosing subgraph. In this way, the computation graph is shown in the yellow space in Fig.10 and the computation graph of RED-GNN is shown in the green space. We observe that the edges involved in computation is the same in different layers. Even though attention is applied in the GNN framework, how the weights cooperate in different layers is unclear. Thus they did not provide interpretation and nor can we come up a way to interpret the reasoning results in GraIL. In comparison, the receptive field in RED-GNN can naturally be traced back from the answer entity e_a to e_q to obtain the pruned r-digraph. As is shown in Sect. C, the attention weight on edges can be used to extract an interpretable subgraph.

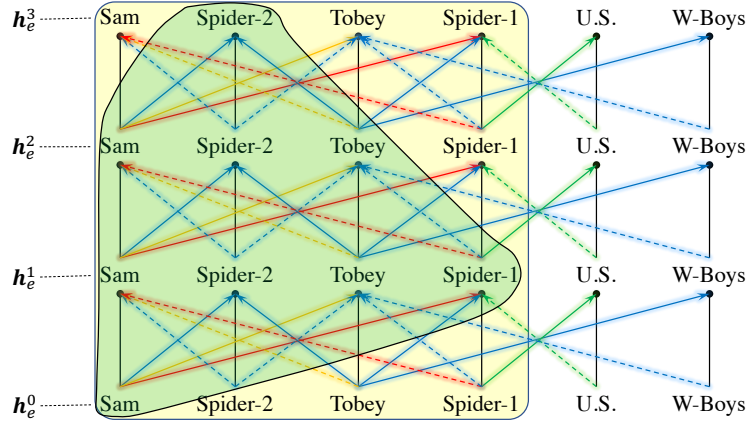


Figure 10: Comparison on the computation graph between GraIL (yellow space) and RED-GNN (green space).

D.3 Empirical evidence

To show that GraIL fails to learn the relational structures, we conduct a tiny ablation study here. Specifically, we change the message function in GraIL from

$$\mathbf{a}_t^k = \sum_{r=1}^R \sum_{s \in \mathcal{N}_r(t)} \alpha_{r,t,s,t}^k \mathbf{W}_r^k \mathbf{h}_s^{k-1},$$

to

$$\mathbf{a}_t^k = \sum_{r=1}^R \sum_{s \in \mathcal{N}_r(t)} \alpha_{r,t,s,t}^k \mathbf{W}^k \mathbf{h}_s^{k-1},$$

where $\alpha_{r,t,s,t}^k = \text{MLP}(\mathbf{h}_s^{k-1}, \mathbf{h}_t^{k-1}, \mathbf{e}_{r_t}^a)$. This procedure removes the relation when aggregating edges to only focus on the homogeneous graph structures.

We name this as GraIL-w.o.-rel. The results on WN18RR (V1), FB15k-237 (V1) and NELL-995 (V1) are shown in Tab.9. We observe that the performance decay is really marginal if relation is removed in the edges. This means that GraIL mainly learns to tell different triples apart by the graph structures and the relation information plays little information. Thus, we claim that GraIL fails to learn the relational dependency in the ill-defined enclosing subgraph.

In comparison, we also change the aggregation function in RED-GNN from (3) to

$$\mathbf{h}_{e_o}^\ell(e_q, r_q) = \delta \left(\mathbf{W}^\ell \cdot \sum_{(e_s, r, e_o) \in \hat{\mathcal{E}}_{e_q}^\ell} \alpha_{e_s, r_q}^\ell (\mathbf{h}_{e_s}^{\ell-1}(e_q, r_q) + \mathbf{v}^\ell) \right),$$

where $\mathbf{v}^\ell \in \mathbb{R}^d$ is shared in the same layer, to remove the relation on edges. We denote this variant as RED-GNN w.o. rel. Note that RED-GNN-w.o.-rel is different from the variant Attn-w.o.- r_q in Tab.3. As in Tab.9, the performance drops dramatically. RED-GNN mainly relies on the relational dependencies in edges as evidence for reasoning.

Table 9: Comparison of GraIL with and without relation information. Evaluated by MRR.

methods	WN18RR (V1)	FB15k-237 (V1)	NELL-995 (V1)
GraIL w.o. rel	0.620	0.255	0.475
GraIL	0.627	0.279	0.481
RED-GNN-w.o.-rel	0.557	0.198	0.384
RED-GNN	0.701	0.369	0.637

E Proofs

E.1 Proposition 4.1

We prove this proposition from the bi-directions such that $\cup_{e_a \in \mathcal{V}} \mathcal{E}_{e_q, e_a|L}^\ell \subseteq \hat{\mathcal{E}}_{e_q}^\ell$ and $\hat{\mathcal{E}}_{e_q}^\ell \subseteq \cup_{e_a \in \mathcal{V}} \mathcal{E}_{e_q, e_a|L}^\ell$.

Proof. First, we prove that $\cup_{e_a \in \mathcal{V}} \mathcal{E}_{e_q, e_a|L}^\ell \subseteq \hat{\mathcal{E}}_{e_q}^\ell$.

As in step-7 of Algorithm 1, $\mathcal{E}_{e_q, e_a|L}^\ell$ is defined as $\mathcal{E}_{e_q, e_a|L}^\ell = \{(e_s, r, e_o) \in \hat{\mathcal{E}}_{e_q}^\ell | e_o \in \mathcal{V}_{e_q, e_a|L}^\ell\}$. Thus we have $\mathcal{E}_{e_q, e_a|L}^\ell \subseteq \hat{\mathcal{E}}_{e_q}^\ell$ and also $\cup_{e_a \in \mathcal{V}} \mathcal{E}_{e_q, e_a|L}^\ell \subseteq \hat{\mathcal{E}}_{e_q}^\ell$.

Second, we prove that $\hat{\mathcal{E}}_{e_q}^\ell \subseteq \cup_{e_a \in \mathcal{V}} \mathcal{E}_{e_q, e_a|L}^\ell$.

We use proof by contradiction here. Assume that $\hat{\mathcal{E}}_{e_q}^\ell \subseteq \cup_{e_a \in \mathcal{V}} \mathcal{E}_{e_q, e_a|L}^\ell$ is wrong, then there must exist $(e_s, r, e_o) \in \hat{\mathcal{E}}_{e_q}^\ell$ and $(e_s, r, e_o) \notin \mathcal{E}_{e_q, e_a|L}^\ell : \forall e_a \in \mathcal{V}$. In other words, there exists an edge (e_s, r, e_o) that can be visited in ℓ steps walking from e_q , but not in any r-digraph $(e_s, r, e_o) \notin \mathcal{E}_{e_q, e_a|L}^\ell$. Based on Def. 3 of r-digraph, then, (e_s, r, e_o) will be an edge that is ℓ steps away from e_q but does not belong to the ℓ -th triple of any relational paths $e_q \rightarrow_{r^1} \rightarrow_{r^2} \dots \rightarrow_{r^L} e_a$, this is impossible. Therefore, we have $\hat{\mathcal{E}}_{e_q}^\ell \subseteq \cup_{e_a \in \mathcal{V}} \mathcal{E}_{e_q, e_a|L}^\ell$.

Based on above two directions, we prove that $\hat{\mathcal{E}}_{e_q}^\ell = \cup_{e_a \in \mathcal{V}} \mathcal{E}_{e_q, e_a|L}^\ell$. □

E.2 Proposition 4.2

Given a certain query triple (e_q, r_q, e_a) and L , when $\mathcal{G}_{e_q, r_q|L} = \emptyset$, it is obvious that $\mathbf{h}_{e_a}^L(e_q, r_q) = \mathbf{0}$ in both Algorithm 1 and Algorithm 2. For $\mathcal{G}_{e_q, r_q|L} \neq \emptyset$, we prove this proposition by induction. We denote $\hat{\mathbf{h}}_e^\ell(e_q, r_q)$ as the representations learned by Algorithm 1 and $\check{\mathbf{h}}_e^\ell(e_q, r_q)$ as the representations learned by Algorithm 2. Then, we show that $\hat{\mathbf{h}}_e^\ell(e_q, r_q) = \check{\mathbf{h}}_e^\ell(e_q, r_q)$ for all $\ell = 1 \dots L$ and $e \in V_{e_q, e_a|L}^\ell$.

Proof. • When $\ell = 1$,

$$\hat{\mathbf{h}}_e^1(e_q, r_q) = \delta(\mathbf{W}^1 \cdot \sum_{(e_q, r, e) \in \mathcal{E}_{e_q, e_a|L}^1} \phi(\mathbf{0}, \mathbf{h}_r^1)),$$

and

$$\check{\mathbf{h}}_e^1(e_q, r_q) = \delta(\mathbf{W}^1 \cdot \sum_{(e_q, r, e) \in \mathcal{E}_{e_q}^1} \phi(\mathbf{0}, \mathbf{h}_r^1)),$$

for $e \in V_{e_q, e_a|L}^1$. It is obvious that $\{(e_q, r, e) \in \mathcal{E}_{e_q, e_a|L}^1\} \equiv \{(e_q, r, e) \in \mathcal{E}_{e_q}^1 | e \in V_{e_q, e_a|L}^1\}$. Thus, we have $\hat{\mathbf{h}}_e^1(e_q, r_q) = \check{\mathbf{h}}_e^1(e_q, r_q)$ for all $e \in V_{e_q, e_a|L}^1$.

- Assume that $\hat{\mathbf{h}}_e^{\ell-1}(e_q, r_q) = \check{\mathbf{h}}_e^{\ell-1}(e_q, r_q)$ for all $e \in V_{e_q, e_a|L}^{\ell-1}$, we prove that $\hat{\mathbf{h}}_e^\ell(e_q, r_q) = \check{\mathbf{h}}_e^\ell(e_q, r_q)$ for all $e \in V_{e_q, e_a|L}^\ell$.

For Algorithm 1, we have

$$\hat{\mathbf{h}}_e^\ell(e_q, r_q) = \delta(\mathbf{W}^\ell \cdot \sum_{(e_s, r, e) \in \mathcal{E}_{e_q, e_a|L}^\ell} \phi(\hat{\mathbf{h}}_{e_s}^{\ell-1}(e_q, r_q), \mathbf{h}_r^\ell)). \quad (6)$$

For Algorithm 2, we have

$$\check{\mathbf{h}}_e^\ell(e_q, r_q) = \delta(\mathbf{W}^\ell \cdot \sum_{(e_s, r, e) \in \hat{\mathcal{E}}_{e_q}^\ell} \phi(\check{\mathbf{h}}_{e_s}^{\ell-1}(e_q, r_q), \mathbf{h}_r^\ell)). \quad (7)$$

As in step 7 of Algorithm 1, $\mathcal{E}_{e_q, e_a|L}^\ell = \{(e_s, r, e_o) \in \hat{\mathcal{E}}_{e_q}^\ell | e_o \in V_{e_q, e_a|L}^\ell\}$. Then, for $e \in V_{e_q, e_a|L}^\ell$, the ranges of summation in (6) and (7) are the same, i.e., $\{(e_s, r, e) \in \mathcal{E}_{e_q, e_a|L}^\ell\} \equiv \{(e_s, r, e) \in \hat{\mathcal{E}}_{e_q}^\ell | e \in V_{e_q, e_a|L}^\ell\}$ and e_s here are all belonging to $V_{e_q, e_a|L}^{\ell-1}$. Hence, based on the assumption, we have $\hat{\mathbf{h}}_e^\ell(e_q, r_q) = \check{\mathbf{h}}_e^\ell(e_q, r_q)$ or all $e \in V_{e_q, e_a|L}^\ell$.

By induction, we can have $\hat{\mathbf{h}}_e^\ell(e_q, r_q) = \check{\mathbf{h}}_e^\ell(e_q, r_q)$ for all $\ell = 1 \dots L$ and $e \in V_{e_q, e_a|L}^\ell$. Therefore, the representation $\hat{\mathbf{h}}_{e_a}^\ell(e_q, r_q)$ and $\check{\mathbf{h}}_{e_a}^\ell(e_q, r_q)$ learned by Algorithm 1 and Algorithm 2, respectively, are identical. \square

E.3 Theorem 4.3

Proof. Based on Def. 3, any set \mathcal{P} of relational paths $e_q \rightarrow_{r_i^1} \rightarrow_{r_i^2} \dots \rightarrow_{r_i^L} e_a$ are contained in the r-digraph $\mathcal{G}_{e_q, e_a|L}$.

Denote $G_{\mathcal{P}}$ as the r-digraph constructed by \mathcal{P} . In each layer, the attention weight is computed as

$$\begin{aligned} \alpha_{e_s, r, r_q}^\ell &= \sigma\left((\mathbf{w}_\alpha^\ell)^\top \text{ReLU}(\mathbf{W}_\alpha^\ell \cdot (\mathbf{h}_{e_s}^{\ell-1}(e_q, r_q) \oplus \mathbf{h}_r^\ell \oplus \mathbf{h}_{r_q}^\ell))\right) \\ &= \text{MLP}^\ell(e_s, r, e_q, r_q). \end{aligned}$$

Then, we prove that $G_{\mathcal{P}}$ can be extracted from the L -th layer and recursively to the first layer.

- In the L -th layer, denote \mathcal{T}_+^L as the set of the triples (e_s, r_i^L, e_a) , whose attention weights are $\alpha_{e_s, r_i^L, r_q}^L = \text{MLP}^L(e_s, r_i^L, r_q, e_q)$, in the L -th layer of $G_{\mathcal{P}}$. Based on the universal approximation theorem [11], there exists a set of parameters $\mathbf{w}_\alpha^L, \mathbf{W}_\alpha^L, \mathbf{h}_r^L$ that can learn a decision boundary θ that $(e_s, r_i^L, e_a) \in \mathcal{T}_+^L$ if $\alpha_{e_s, r_i^L, r_q}^L > \theta$ and otherwise $(e_s, r_i^L, e_a) \notin \mathcal{T}_+^L$. Then the L -th layer of $G_{\mathcal{P}}$ can be extracted.

- Similarly, denote \mathcal{T}_+^{L-1} as the set of the triples (e_s, r_i^{L-1}, e_o) that connects with the remaining entities in the $L - 1$ -th layer. Then, there also exists a set of parameters $\mathbf{w}_\alpha^{L-1}, \mathbf{W}_\alpha^{L-1}, \mathbf{h}_r^{L-1}$ that can learn a decision boundary θ that $(e_s, r_i^{L-1}, e_o) \in \mathcal{T}_+^{L-1}$ if $\alpha_{e_s, r_i^{L-1}, r_q}^{L-1} > \theta$ and otherwise not in. Besides, $\mathbf{w}_\alpha^{L-1}, \mathbf{W}_\alpha^{L-1}, \mathbf{h}_r^{L-1}$ and $\mathbf{w}_\alpha^L, \mathbf{W}_\alpha^L, \mathbf{h}_r^L$ are independent with each other. Thus, we can extract the $L - 1$ -th layer of $\mathcal{G}_\mathcal{P}$.
- Finally, with recursive execution, $\mathcal{G}_\mathcal{P}$ can be extracted as the subgraph in $\mathcal{G}_{e_q, e_a|L}$ with attention weights $\alpha_{e_s, r, r_q}^\ell > \theta$.

□